CARBON 47 (2009) 1617–1628

available at www.sciencedirect.com

ScienceDirect

journal homepage: www.elsevier.com/locate/carbon

Quenched solid density functional theory and pore size analysis of micro-mesoporous carbons

Alexander V. Neimark[a,*], *Yangzheng Lin*[a], *Peter I. Ravikovitch*[b], *Matthias Thommes*[c]

[a]*Rutgers University, Chemical and Biochemical Engineering, 98 Brett Road, Piscataway, NJ 08854, United States*
[b]*ExxonMobil Research and Engineering, Annandale, NJ 08801, United States*
[c]*Quantachrome Instruments, Boynton Beach, FL 33426, United States*

ARTICLE INFO

Article history:
Received 10 December 2008
Accepted 27 January 2009
Available online 13 February 2009

ABSTRACT

We present a new model of adsorption on micro-mesoporous carbons based on the quenched solid density functional theory (QSDFT). QSDFT quantitatively accounts for the surface geometrical inhomogeneity in terms of the roughness parameter. We developed the QSDFT models for pore size distribution calculations in the range of pore widths from 0.4 to 35 nm from nitrogen at 77.4 K and argon at 87.3 K adsorption isotherms. The QSDFT model improves significantly the method of adsorption porosimetry: the pore size distribution (PSD) functions do not possess gaps in the regions of ~1 nm and ~2 nm, which are typical artifacts of the standard non-local density functional theory (NLDFT) model that treats the pore walls as homogeneous graphite-like plane surfaces. The advantages of the QSDFT method are demonstrated on various carbons, including activated carbons fibers, coal based granular carbon, water purification adsorbents, and mirco-mesoporous carbon CMK-1 templated on MCM-48 silica. The results of PSD calculations from nitrogen and argon are consistent, however, argon adsorption provides a better resolution of micropore sizes at low vapor pressures than nitrogen adsorption.

1. Introduction

Over the last decade, a significant progress has been achieved in understanding the underlying mechanisms of adsorption in micro- and mesoporous solids and, consequently, in elaborating the theoretical foundations of adsorption characterization. This progress has been related, to a large extent, to the application of microscopic methods such as the density functional theory (DFT) of inhomogeneous fluids, which allows one to describe adsorption and phase behavior of fluids in pores on a molecular level [1–3]. DFT has helped qualitatively classify the specifics of adsorption and capillary condensation in pores of different geometries [2,4–6]. It has been shown that the non-local density functional theory (NLDFT) with suitably chosen parameters of fluid–fluid and fluid–solid interactions quantitatively predicts the positions of capillary condensation and evaporation transitions of argon and nitrogen in cylindrical and spherical pores of ordered mesoporous molecular sieves such as MCM-41, SBA-15, SBA-16, and hierarchically structured silica materials [7–9]. The NLDFT method has been commercialized by the producers of adsorption equipment for the interpretation of experimental data and the pore size distribution (PSD) calculation from adsorption isotherms. The NLDFT method is widely applied, and it is featured in a recent standard by ISO [10].

While NLDFT has been demonstrated to be a reliable method for characterization of ordered silica materials, pore size analysis of carbons remains difficult. Although the first DFT methods were suggested for activated carbons [11–13],

* *Corresponding author*:
E-mail address: aneimark@rutgers.edu (A.V. Neimark).
0008-6223/$ - see front matter © 2009 Elsevier Ltd. All rights reserved.
doi:10.1016/j.carbon.2009.01.050

the inherent complexity and heterogeneity of pore structures in carbonaceous materials make the development of improved adsorption isotherm models and new characterization methods a topical problem. Current implementations of NLDFT for carbon materials are based on a model of independent slit-shaped pores with ideal graphitic walls. Such a model has a significant drawback; starting from pore widths of more than a few molecular diameters, theoretical adsorption isotherms exhibit multiple steps associated with layering transitions related to the formation of a monolayer, second adsorbed layer, and so on [14–16]. Experimentally, stepwise adsorption isotherms are observed only at low temperatures for fluids adsorbed onto molecularly smooth surfaces, such as mica or graphite. However, in disordered carbon materials (e.g. active carbons, activated carbon fibers, etc.), layering transitions are hindered due to inherent energetic and geometrical heterogeneities of real surfaces. The layering steps on the theoretical isotherms cause artificial gaps on the calculated pore size distributions, because the computational scheme, which fits the experimental isotherm as a linear combination of the theoretical isotherms in individual pores, attributes a layering step to a pore filling step in a pore of a certain size. For example, in the case of nitrogen at 77.4 K on graphite, the monolayer formation step in NLDFT occurs at the same relative pressure of $\sim 0.3 \times 10^{-4}\, p/p_0$ as the pore filling in ~1 nm wide slit. This coincidence results in a prominent false gap on the pore size distribution histograms [15,16]. The second false gap around ~2 nm may appear due to the artificial first-to-second layer transition predicted by NLDFT at $\sim 0.2\, p/p_0$. This mismatch between the theoretical assumption of a smooth and homogeneous surface and the experimental situation is especially pronounced for materials with broad PSDs that is typical for many microporous carbons (see detailed discussion with examples below). It is characteristic for novel nanoporous carbons, which were specifically designed for pore size sensitive applications, such as carbide derived carbons [17,18] and exfoliated graphite nanofibers [19]. In addition, the fit of the low-pressure part of experimental isotherms is rarely satisfactory – calculated isotherms exhibit unavoidable swings reflecting layering transitions, see examples given in Section 4).

Several approaches were suggested to account for the heterogeneity of carbon materials. New molecular structural models of porous carbons have been developed by reverse Monte Carlo techniques [20,21]. Although very promising, these models are still too complex to be implemented for routine pore size analyses. Within the framework of the standard slit-pore model of carbons, a variability of pore wall thickness has been introduced [22–24a,b], but it led to just a marginal improvement over the standard NLDFT approach [16]. Molecular simulations have demonstrated that the surface roughness and defects affect significantly the shape of adsorption isotherms on heterogeneous surfaces [25–27]. In particular, Do and Do [27] simulated argon adsorption on the surfaces of carbon blacks and achieved quantitative agreement with experimental data by introducing various levels and sizes of surface defects. Several modifications of the solid–fluid potential within the Tarazona's version of NLDFT were proposed [14,28] to account effectively for the surface heterogeneity and generate smoothened adsorption isotherms. Ustinov et al. [28] developed a model for the pore size analysis of carbons, which is based on a fit to the reference isotherm on nongraphitized carbon black.

Recently, two of us have suggested the quenched solid density functional theory (QSDFT) [29]. QSDFT was devised for modeling adsorption in heterogeneous materials with corrugated amorphous walls. It has been successfully applied to siliceous materials of MCM-41 and SBA-15 type [29]. QSDFT is a multicomponent DFT, in which the solid is treated as one of the components of adsorbate–adsorbent system. In contrast to the conventional NLDFT models that assumed structureless graphitic pore walls, the solid is modeled using the distribution of solid atoms rather than the source of the external potential field. OSDFT allows one to account explicitly for the effects of surface heterogeneity. The surface heterogeneity in the QSDFT model is characterized by a single roughness parameter that represents the characteristic scale of surface corrugation.

In this work, the QSDFT approach is extended to adsorption of nitrogen at 77.4 K and argon at 87.3 K on carbon adsorbents. Although nitrogen adsorption is traditionally considered as a standard technique for pore size characterization, argon adsorption at 87.3 K has advantages for ultra-microporous materials, since argon fills micropores of dimensions <0.7 nm at higher pressures than nitrogen at 77.4 K that leads to faster adsorption kinetics and allows one to obtain high resolution low pressure adsorption isotherms [30]. The paper is structured as follows. In Section 2, we describe the basic equations of the QSDFT model and its parameters. It is worth noting that the QSDFT model is capable of describing adsorption isotherms on carbon materials with various degree of pore wall roughness/corrugation and/or surface defects. The roughness parameter and the fluid–solid interaction parameters can be customized for a given class of carbons by fitting the reference experimental adsorption isotherm on a well-characterized reference surface, e.g., on graphitized and non-graphitized carbon blacks [31–34]. In this work, we have chosen Cabot BP-280 carbon black with a partial degree of graphitization [33,34] as the reference surface. The characteristic features of adsorption on the reference surface and capillary condensation in pores with molecularly rough walls are presented in Section 3. We show that the QSDFT model quantitatively describes adsorption of nitrogen and argon on Cabot BP-280 carbon black, and that QSDFT adsorption isotherms do not exhibit layering transitions. We developed the QSDFT models for pore size distribution calculations in the range of pore widths from 0.4 to 35 nm. The QSDFT model improves significantly the method of adsorption porosimetry: the pore size distribution (PSD) functions do not possess artificial gaps in the regions of ~1 nm and ~2nm, which are typical artifacts of the standard NLDFT model that treats the pore walls as homogeneous graphite-like plane surfaces. The validity of the QSDFT method is demonstrated in Section 4 on various carbons, including activated carbons fibers, coal based granular carbon, water filtration adsorbents, and mirco-mesoporous CMK-1 carbon templated on MCM-48 silica. The results of PSD calculations from nitrogen and argon are consistent, however, argon adsorption provides a better resolution of

micropore sizes at low vapor pressures than nitrogen adsorption. Conclusions are summarized in Section 5. Additional examples of calculations are given in Supplementary Information.

2. QSDFT model for adsorption on carbons

2.1. Basic formulation of QSDFT

The density functional theory implies that at the conditions of thermodynamic equilibrium the spatial distribution of adsorbed species corresponds to the minimum of the grand thermodynamic potential at given chemical potential(s), pore volume and temperature. The QSDFT model [29] is based on the multicomponent density functional theory method, in which the grand thermodynamic potential Ω is defined as

$$\Omega[\{\rho_i(\mathbf{r})\}] = F_{int}[\{\rho_i(\mathbf{r})\}] + \sum_i \int d\mathbf{r}\rho_i(\mathbf{r})[\psi_i(\mathbf{r}) - \mu_i] \quad (1)$$

where F_{int} is the intrinsic Helmholtz free energy, ρ_i and μ_i are the local number density and chemical potential of component i, and ψ_i are the local external potentials.

In the QSDFT model of single component adsorption, we consider solid as a quenched component of the two-component solid–fluid system. The adsorption interactions are reduced to the pairwise interactions between molecules of adsorbate (fluid) and adsorbent (solid), and external potentials are not considered. Thus, the grand thermodynamic potential is reduced to

$$\Omega[\rho_s(\mathbf{r});\rho_f(\mathbf{r})] = F_{int}[\rho_s(\mathbf{r});\rho_f(\mathbf{r})] - \mu_s \int d\mathbf{r}\rho_s(\mathbf{r}) - \mu_f \times \int d\mathbf{r}\rho_f(\mathbf{r}) \quad (2)$$

The minimization of the grand thermodynamic potential is performed with respect to the fluid density $\rho_f(\mathbf{r})$ keeping the solid density $\rho_s(\mathbf{r})$ and the contributions form solid–solid atomic interactions unchanged: $\delta\Omega[\rho_s(\mathbf{r});\rho_f(\mathbf{r})]/\delta\rho_f(\mathbf{r}) = 0$, which yields the Euler equation

$$\delta F_{int}[\rho_s(\mathbf{r});\rho_f(\mathbf{r})]/\delta\rho_f(\mathbf{r}) - \mu_f = 0 \quad (3)$$

The intrinsic Helmholtz free energy is conventionally divided into ideal and excess parts,

$$F_{int}[\rho_s(\mathbf{r});\rho_f(\mathbf{r})] = F_{id}[\rho_s(\mathbf{r});\rho_f(\mathbf{r})] + F_{ex}[\rho_s(\mathbf{r});\rho_f(\mathbf{r})] \quad (4)$$

with the ideal gas free energy given by exact expressions,

$$F_{id}[\rho_s(\mathbf{r});\rho_f(\mathbf{r})] = k_BT \int d\mathbf{r}\rho_s(\mathbf{r})\{\ln[\rho_s(\mathbf{r})\Lambda_s^3] - 1\} + k_BT \times \int d\mathbf{r}\rho_f(\mathbf{r})\{\ln[\rho_f(\mathbf{r})\Lambda_f^3] - 1\} \quad (5)$$

where k_B is the Boltzman constant, T is the absolute temperature, and Λ is the de Broglie wavelength.

The excess part of the Helmholtz free energy is expressed in terms of short-range repulsion and long-range van der Waals attraction. The short range hard-core repulsion is represented by the excess free energy potential of the hard sphere (HS) mixture $F_{ex}^{hs}[\rho_s(\mathbf{r});\rho_f(\mathbf{r})]$, and the attractive part of the Helmholtz free energy is calculated in a mean field fashion:

$$\begin{aligned} F_{ex}[\rho_s(\mathbf{r});\rho_f(\mathbf{r})] = {} & F_{ex}^{hs}[\rho_s(\mathbf{r});\rho_f(\mathbf{r})] \\ & + \frac{1}{2}d\mathbf{r}d\mathbf{r}'\rho_s(\mathbf{r})\rho_s(\mathbf{r}')u_{ss}^{att}(|\mathbf{r}-\mathbf{r}'|) \\ & + \frac{1}{2}d\mathbf{r}d\mathbf{r}'\rho_f(\mathbf{r})\rho_f(\mathbf{r}')u_{ff}^{att}(|\mathbf{r}-\mathbf{r}'|) \\ & + d\mathbf{r}d\mathbf{r}'\rho_s(\mathbf{r})\rho_f(\mathbf{r}')u_{sf}^{att}(|\mathbf{r}-\mathbf{r}'|) \end{aligned} \quad (6)$$

where u^{att} are the attractive potentials of fluid–fluid, fluid–solid, and solid–solid interactions treated in a symmetric manner. That is, the solid is modeled as a compound of hardcore spheres, interacting with the fluid molecules via the pairwise attractive potential $u_{sf}(r)$. The Euler equation (3) is re-written as

$$k_BT\ln[\rho_f(\mathbf{r})\Lambda^3] + \frac{\delta F_{ex}^{hs}[\rho_s(\mathbf{r});\rho_f(\mathbf{r})]}{\delta\rho_f(\mathbf{r})} + \int d\mathbf{r}'\rho_f(\mathbf{r}')u_{ff}^{att}(|\mathbf{r}-\mathbf{r}'|) + \int d\mathbf{r}'\rho_s(\mathbf{r}')u_{sf}^{att}(|\mathbf{r}-\mathbf{r}'|) - \mu_f = 0 \quad (7)$$

Note, that the bulk fluid density and the chemical potential are related through the bulk equation of state,

$$\mu_f = k_BT\ln(\rho_f\Lambda^3) + \mu_{ex}^{hs}(\rho_f) + \rho_f\int d\mathbf{r}'u_{ff}^{att}(|\mathbf{r}-\mathbf{r}'|) \quad (8)$$

The key term in the QSDFT model is $F_{ex}^{hs}[\rho_s(\mathbf{r});\rho_f(\mathbf{r})]$ – the excess free energy of the solid–fluid HS mixture. In this work, we employ the fundamental measure theory (FMT) of Rosenfeld [35], which can be easily applied for mixtures. Several modifications of FMT were recommended in the literature [36–38]. We adopted the RLST version of FMT [38], which is consistent with the Percus–Yevick (PY) equation of state for the bulk HS fluid,

$$F_{ex}^{hs}[\{\rho_i(\mathbf{r})\}] = k_BT\int d\mathbf{r}\left\{-n_0\ln(1-n_3) + \frac{n_1n_2 - \mathbf{n}_{V1}\mathbf{n}_{V2}}{1-n_3} + \frac{n_2^3}{24\pi(1-n_3)^2}(1-3\xi^2+2\xi^3)\right\} \quad (9)$$

where $\xi = |\mathbf{n}_{V2}/n_2|$ and $\{n_\alpha\}$ denote the system averaged fundamental geometric measures of the particles,

$$n_\alpha(\mathbf{r}) = \sum_i \int d\mathbf{r}'\rho_i(\mathbf{r}')w_i^{(\alpha)}(\mathbf{r}-\mathbf{r}') \quad (10)$$

The weight functions $w_i^{(\alpha)}$ characterize the geometry of the hard sphere particles. In 3-dimensional consideration, four scalar functions are related to the surface and volume,

$$w_i^{(0)}(\mathbf{r}) = \frac{\delta(R_i-r)}{4\pi R_i^2},\ w_i^{(1)}(\mathbf{r}) = \frac{\delta(R_i-r)}{4\pi R_i},\ w_i^{(2)}(\mathbf{r}) = \delta(R_i-r),\ w_i^{(3)}(\mathbf{r}) = \Theta(R_i-r) \quad (11)$$

and two vector functions characterize the variance across the particle surface

$$\mathbf{w}_i^{(V1)}(\mathbf{r}) = (\mathbf{r}/r)\frac{\delta(R_i-r)}{4\pi R_i}, \mathbf{w}_i^{(V2)}(\mathbf{r}) = (\mathbf{r}/r)\delta(R_i-r) \quad (12)$$

In Eqs. (11) and (12), R_i is the hard-sphere radius, $\delta(r)$ is the Dirac delta function, and $\Theta(r)$ is the Heaviside step function.

In the bulk fluid, the excess hard sphere chemical potential is calculated by the PY equation,

$$\mu_{ex}^{hs} = k_BT\left[-\ln(1-\eta) + \eta\frac{14-13\eta+5\eta^2}{2(1-\eta)^3}\right] \quad (13)$$

where $\eta = \frac{\pi}{6}\rho_f d_{hs}^3$ is the packing fraction and d_{hs} is the hard sphere diameter of the fluid molecules.

2.2. Parameters of intermolecular interactions

Lennard-Jones potential was used to represent both fluid–fluid and fluid–solid interactions. The standard WCA scheme was adopted to calculate the van der Waals attraction potentials.

$$u_{ij}^{att}(r) = \begin{cases} -\varepsilon_{ij} & r \leqslant 2^{1/6}\sigma_{ij} \\ 4\varepsilon_{ij}[(\sigma_{ij}/r)^{12} - (\sigma_{ij}/r)^{6}] & r > 2^{1/6}\sigma_{ij} \end{cases} \quad (14)$$

For N_2–N_2 interaction, $\varepsilon_{ff}/k_B = 95.77$ K, $\sigma_{ff} = d_{HS} = 0.3549$ nm; for Ar–Ar interaction, $\varepsilon_{ff}/k_B = 111.95$ K, $\sigma_{ff} = d_{HS} = 0.3358$ nm [29]. These values were fitted to reproduce the bulk properties of adsorbates at its boiling temperature. Note that these values are slightly different from nitrogen model used in NLDFT [16] because QSDFT uses PY equation for hard spheres while NLDFT uses Carnahan–Starling equation.

The effective LJ parameters for solid–fluid interactions were chosen as follows. For Carbon–N_2 interaction $\varepsilon_{sf}/k_B = 150$ K, $\sigma_{sf} = 0.269$ nm, and for Carbon–Ar $\varepsilon_{sf}/k_B = 162.18$ K, $\sigma_{sf} = 0.2595$ nm. The parameters for Carbon–Ar were calculated from the combining rules.

2.3. The model for carbon surface

We have chosen Cabot BP-280 carbon black as a typical example of carbon surface. The surface of BP-280 represents a partially graphitized surface and, therefore, can serve as a suitable reference representative of a wide class of carbon surfaces. We have built the QSDFT model, which reproduces the adsorption behavior of nitrogen and argon on Cabot BP-280. The prominent feature of low temperature adsorption on nonporous graphitized carbons is a monolayer formation step at low pressures. For carbons with progressively lower degree of graphitization, this step becomes less and less pronounced [25,32]. In the QSDFT model, the surface heterogeneity of carbons is effectively characterized by the roughness parameter that represents an average characteristic scale of surface corrugations, as well as slightly decreased density of carbon atoms in the first surface layer. The surface is described by a one-dimensional density profile of carbon atoms in the form of a linear ramp (see Fig. 1) given by

$$\rho_s(z) = \begin{cases} \rho_s^0 & 0 \leqslant z < h_0 \\ 0.75\rho_s^0 \times (1 - \frac{z-h_0}{2\delta}) & h_0 \leqslant z < h_0 + 2\delta \\ 0 & z \geqslant h_0 + 2\delta \end{cases} \quad (15)$$

Here $\rho_s^0 = 0.114$ Å^{-3} is the density of bulk carbon; h_0 is the thickness of the solid wall assumed to be $h_0 = 2 \times 0.34$ nm to conform to experimental observations for typical porous carbons [24b], although we found that the proposed model was not very sensitive to the value of h_0. The hard sphere diameter of carbon atoms is 2.217×10^{-10} m, and is obtained from the assumption of the random packing of carbon atoms. The roughness parameter δ represents the half-width of the density ramp. It was taken as $\delta = 0.13$ nm. The edge position z_e of the solid wall is determined from the condition of zero solid excess,

$$\int_{h_0}^{h_0+2\delta} \rho_s(z)dz = \rho_s^0(z_e - h_0) \quad (16)$$

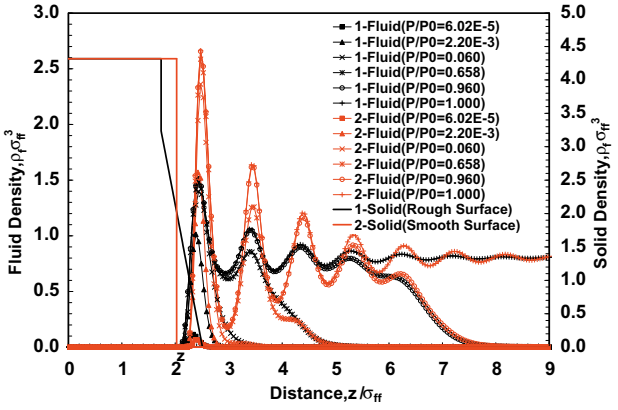

Fig. 1 – Formation of adsorbed layers on molecularly rough surface of Cabot BP-280 carbon black for argon at 87.3 K. Solid density distribution is modeled as a linear ramp, Eq. (12), with the roughness parameter $\delta = 0.13$ nm. Fluid profiles at different relative vapor pressures (insert) show successive stages of adsorption process: filling the surface corrugations, formation of monolayer, and multilayer liquid-like film.

3. Simulation results

3.1. Density profiles and adsorption isotherms on open surface

Solution of the Euler equation (7) gives the fluid density profile at given chemical potential, or relative pressure. Fig. 1 shows the formation of adsorbed layers on molecularly rough surface of Cabot BP-280 carbon black for argon at 87.3 K. The surface roughness is modeled by the linear ramp function (15) with the roughness parameter $\delta = 0.13$ nm. Fluid profiles at different relative vapor pressures (insert) show successive stages of adsorption process: filling the surface corrugations, formation of monolayer, and multilayer liquid-like film. Note, that even such small extent of the surface roughness ($\delta < 0.3\ \sigma_{ff}$) brings about a gradual formation of the monolayer and eliminates a step-wise monolayer transition inherent in the smooth surface models. Transition from the first to second layer is also rather smooth. A similar figure for nitrogen adsorption at 77 K is given in Supplementary Information.

The adsorption isotherm is calculated by integrating the fluid density profile,

$$N = \int_{z_0}^{z_m} \rho_f(z)dz - \rho_{bulk}[z_m - (z_e + \sigma_{sf})] \quad (17)$$

Here, z_m is the maximum distance during the integration. In Fig. 2, we present for a comparison the calculated adsorption isotherms on molecularly rough and step-wise smooth surfaces, which correspond to the example given in Fig. 1. In contrast with the isotherm on the smooth surface, which shows prominent steps associated with the layering transitions, the isotherm on the molecularly rough surface is perfectly smooth. The extend of surface roughness of less then 30% of the fluid molecular diameter is enough to level down the

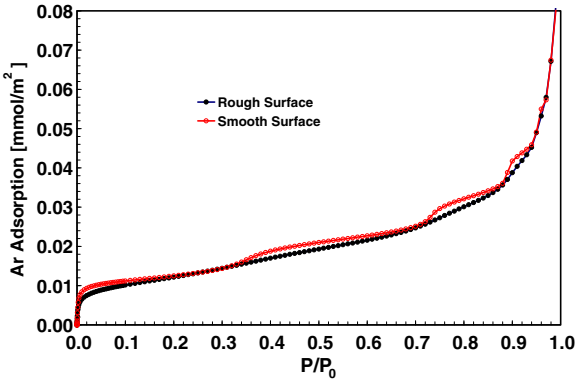

Fig. 2 – Comparison the calculated adsorption isotherms of Ar at 87.3 K on smooth and molecularly rough (the roughness parameter $\delta = 0.13$ nm) surfaces, which correspond to the examples given in Fig. 1.

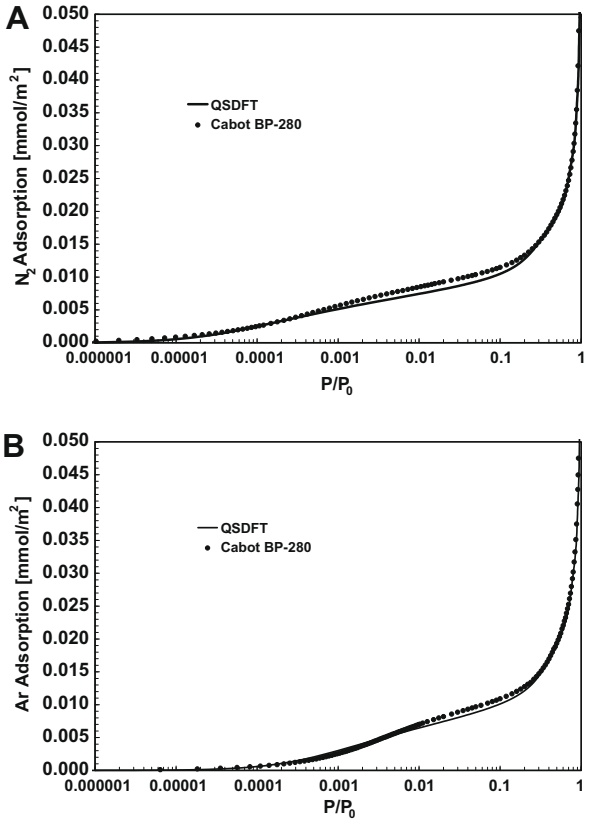

Fig. 3 – Comparison of calculated adsorption isotherms of (A) N_2 at 77.4 K and (B) Ar at 87.3 K on Cabot BP-280 carbon black at 77.4 K (logarithmic scale). Experimental data [33,34].

artificial inflections caused by the packing induced layering. A similar figure for nitrogen adsorption at 77 K is given in Supplementary Information.

The calculated isotherms on nitrogen at 77.4 K and argon at 87.3 K on Cabot BP-280 carbon black are presented in Fig. 3A and B in comparison with the experimental data [33,34]. The calculated isotherms do not exhibit artificial layering transitions characteristic to the NLDFT model with smooth pore wall [16]. Agreement with experiment is quite reasonable taking into account the wide range of vapor pressures from 1 atm down to 10^{-6} atm.

3.2. *Adsorption isotherms in carbon nanopores*

The kernels of equilibrium adsorption isotherms of nitrogen at 77.4 K and argon at 87.3 K have been calculated in slit-shaped pores with molecularly rough walls using the surface model for Cabot BP-280 carbon black in the range of pore

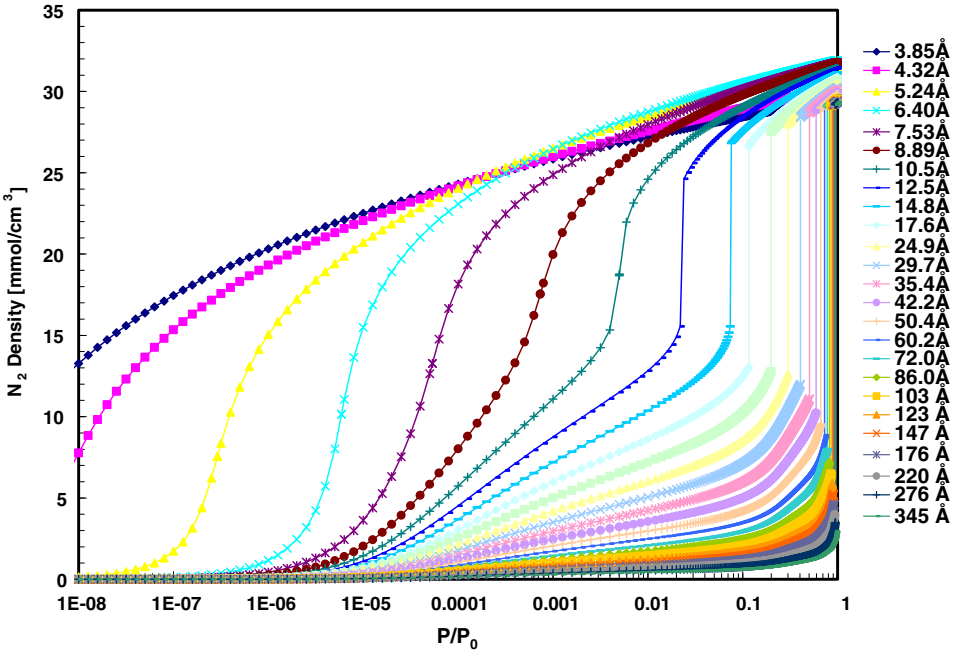

Fig. 4. – Kernel of selected equilibrium adsorption isotherms of nitrogen at 77.4 K in slit-shaped pores with molecularly rough walls using the surface model for Cabot BP-280 carbon black. The pore widths are given in the right panel.

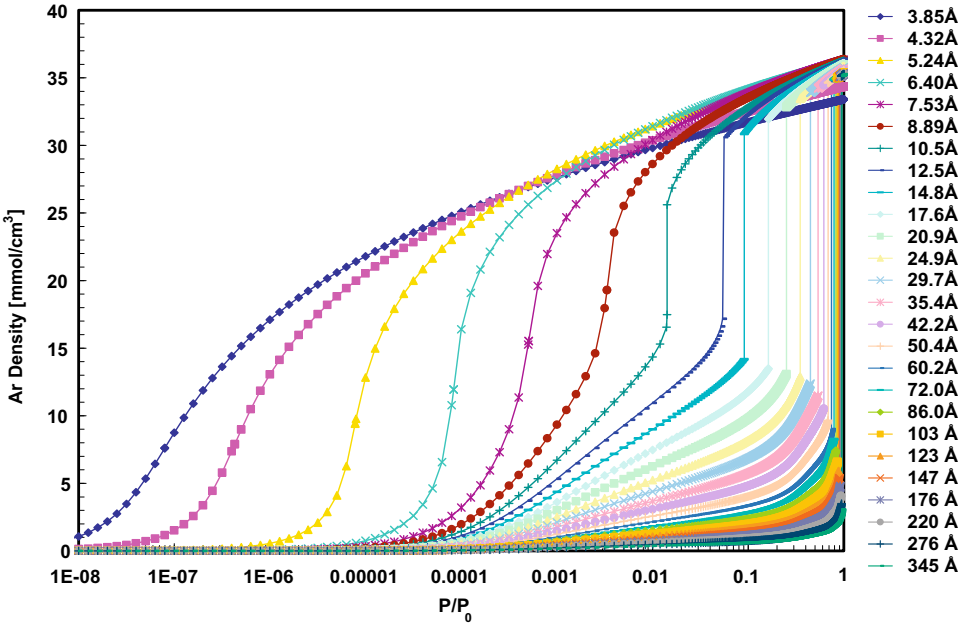

Fig. 5. – Kernel of selected equilibrium adsorption isotherms of argon at 87.3 K in slit-shaped pores with molecularly rough walls using the surface model for Cabot BP-280 carbon black. The pore widths are given in the right panel.

widths w from ~4 to 350 A. Selected isotherms are presented in Figs. 4 and 5.

The isotherm shape depends on the pore size. Adsorption in micropores of width <~10 A is characterized by s-shaped isotherms with a prominent inflection. In micropores of width >~1 nm) and mesopores, the isotherms exhibit a step that corresponds to the equilibrium capillary condensation transition from the adsorbed film to the pore filling. It is worth noting that due to the surface roughness the isotherms prior to the capillary condensation transition are smooth and do not show any steps or inflections.

In the region of capillary condensation, calculated QSDFT isotherms exhibit a hysteretic behavior tracing metastable states along the adsorption and desorption isotherms terminated by stepwise spontaneous capillary condensation and desorption transitions. A typical example of calculated adsorption isotherm in a mesopore (argon adsorption and desorption isotherms at 87.3 K in 3.9 nm pore) is given in Fig. 6. The position of equilibrium capillary condensation is determined form the condition of equality of the grand thermodynamic potentials (2) for the adsorbed film and condensed fluid configurations [1]. The grand thermodynamic potential calculated along the adsorption and desorption branches are presented in the same figure.

Calculated density profiles for selected states along adsorption and desorption isotherms given are presented in Fig. 6. The densities profiles show the formation of mono- and multilayer adsorption film prior to capillary condensation and gradual reduction of adsorbed fluid density during desorption prior to spontaneous evaporation. Note that the density profile oscillations are leveled compared to the smooth wall model (see Fig. 7).

The pore filling pressure is defined either from the position of the isotherm inflection in micropores <~1 nm or from the position of the capillary condensation step in wider pores. The filling pressure strongly depends on the pore width and, thus, can be used for calculating pore size distributions from experimental isotherms. The equilibrium filling pressures of nitrogen and argon for different pore sizes are shown in Figs. 8 and 9.

Argon adsorption has the same qualitative features as nitrogen adsorption, however, the pore filling occurs at higher relative pressures. This shift allows one to assess the smallest pores of 0.4–0.5 nm in widths at measurable relative pressures 10^{-7}–10^{-5} by using argon instead of nitrogen.

3.3. *QSDFT method for pore size distribution calculations*

Based on the kernels of equilibrium isotherms, we developed a new QSDFT method for calculating the pore size distribu-

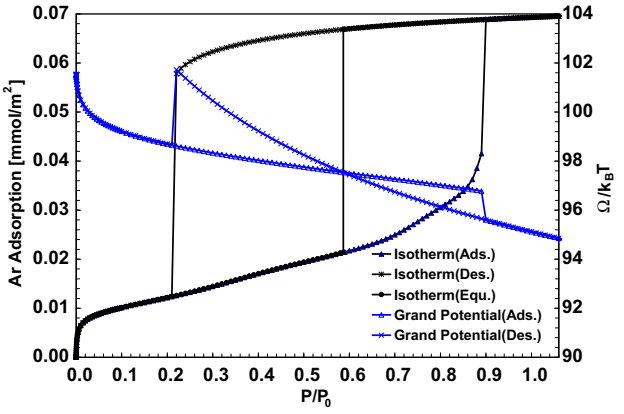

Fig. 6 – Calculated argon adsorption and desorption isotherms at 87.3 K in 3.9 nm mesopore. The position of equilibrium capillary condensation is determined form the condition of equality of the grand thermodynamic potentials along adsorption and desorption branches.

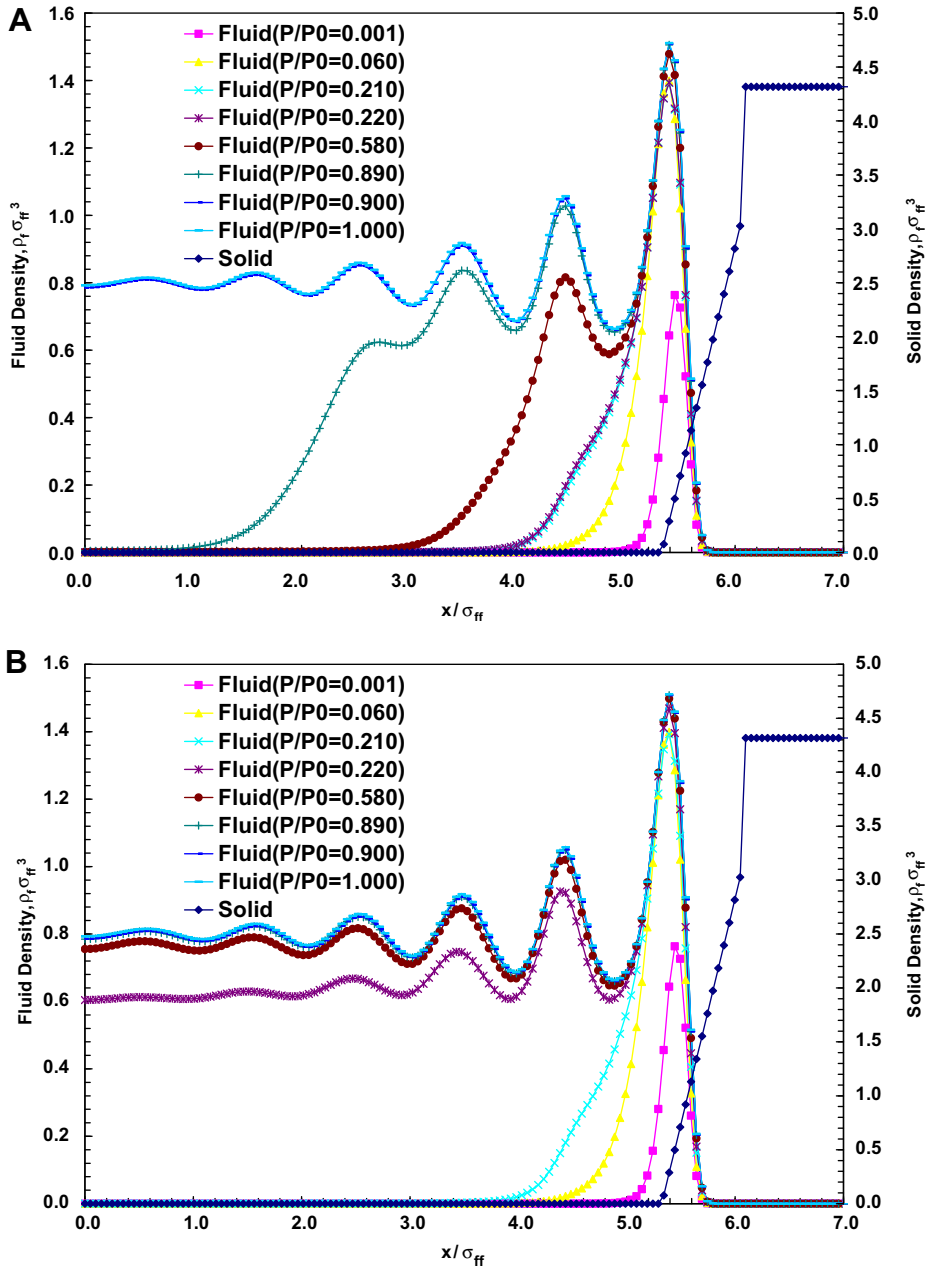

Fig. 7 – Calculated density profiles for selected states along adsorption (A) and desorption (B) isotherms given in Fig. 6 (*x* is the distance from the pore center).

tions in micro-mesoporous carbons from nitrogen and argon adsorption isotherms. The pore size distribution function $f(w)$ is determined from the solution of the integral adsorption equation,

$$N_{exp}(p/p_0) = \int_{H_{min}}^{H_{max}} N_{QSDFT}(p/p_0, w) f(w) dw \quad (18)$$

Here H_{min} and H_{max} the minimum and maximum pore sizes in the kernel. Eq. (18) represents the experimental isotherm as a sum of theoretical isotherms in pores of different sizes taken in proportion with the pore size distribution function.

In the examples presented below, Eq. (18) was solved by the quick non-negative least square (QNNLS) method [16,39]. In this method Eq. (18) is written as a linear matrix equation and solved using an adaptable procedure that combines Tikhonov regularization method with non-negative least squares algorithm (NNLS) [40]. A variant of the so-called L-curve [41] method and an original algorithm are used to automatically choose an optimal regularization parameter that provides an optimal balance between the smoothness of the pore size distribution function and the quality of the fit to the experimental adsorption isotherm.

4. Application examples

We applied the QSDFT model to nitrogen (77.4 K) and argon (87.3 K) adsorption isotherms obtained on some typical carbons, including activated carbons fibers, coal based granular

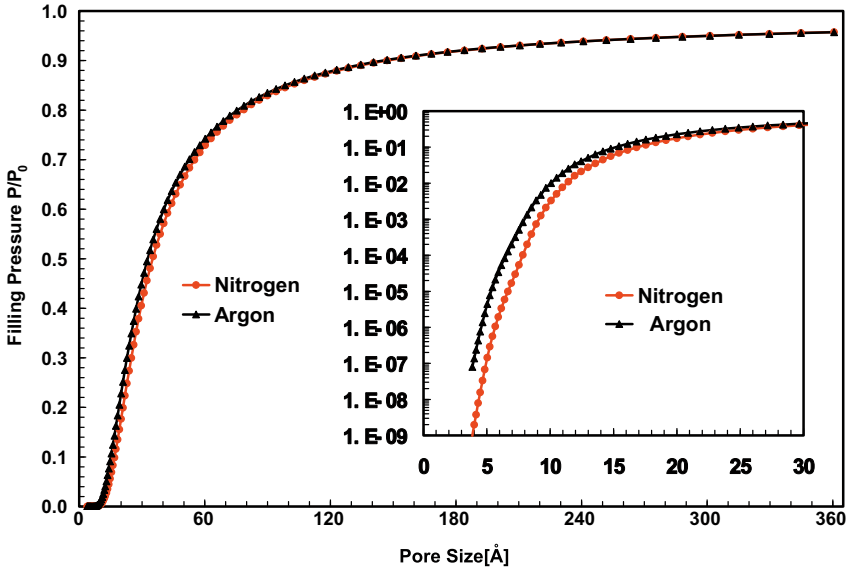

Fig. 8 – Equilibrium filling pressures for nitrogen adsorption at 77.4 K and argon adsorption at 87.3 K in carbon pores.

carbon (Calgon F400), water purification adsorbents such as Norit CM-C2 and CM-E2 carbon (prepared from coconut shell), as well as micro/mesoporous CMK-1 carbon (templated on MCM-48 silica. The active carbon fiber (ACF-15) was obtained from Osaka gas (Japan), Calgon F400 sample was obtained from Australian Water Quality Centre, Adelaide, CMC-2 and CME-2 samples were obtained from Prof. Catherine Morlay (Universite de Lyon, France), and CMK-1 carbon was obtained from Prof. Michael Froeba (University of Hamburg, Germany). High resolution nitrogen (77.4 K) and argon (77.4 K, and 87.3 K) adsorption/desorption isotherm measurements were performed with an Autosorb-I-MP adsorption instrument (Quantachrome Instruments) in the relative pressure range from 1×10^{-7} to 1.

In Fig. 9, we present the pore size distribution calculations for active carbon fiber ACF-15 for the nitrogen adsorption isotherm and compare the QSFDFT and NLDFT results. Fig. 9A shows the fit of the experimental isotherm with the calculated theoretical one. The QSDFT provides a significant improvement in the agreement between the experimental and the theoretical isotherms, in particular in the low pressure range of the micropore filling (Fig. 9A). The prominent step at $p/p_0\sim0.3\times10^{-3}$ that is characteristic to the theoretical NLDFT isotherms, which is due to the monolayer transition on the smooth graphite surface, is completely eliminated in the QSDFT isotherm. As a consequence, a sharp minimum in the NLDFT pore size distribution curve at ~1 nm, which is typical to the NLDFT pore size distribution curves for many microporous carbons, does not appear in QSDFT calculations (Fig. 9B). This confirms that this minimum on the differential NLDFT pore size distribution is indeed an artifact caused by the monolayer step in the NLDFT approach, which occurs at the same pressure as the pore filling in ~1 nm slit pore. The pore size distribution curves in Fig. 11A shows that QSDFT and NLDFT agree beyond the regions where artificial gaps were observed with NLDFT; this is in line with the observation that the cumulative pore volumes calculated by NLDFT and QSDFT (Fig. 9C) are also in good agreement. Similar results for pitch-based activated carbon fiber P10 (experimental data from Ref. [16]) are given in Supplementary Information.

In Fig. 10, we present an example of micro-mesoporous templated carbon CMK-1. This carbon [42,43] exhibits an ordered mesostructure and quite disordered microporosity. Two prominent swings on the NLDFT isotherm seen in Fig. 10A correspond to the monolayer and second layer transitions, which are reflected in two characteristic gaps on the NLDFT differential pore distribution (Fig. 10B) around 1nm and around 2 nm. The QSDFT isotherm nicely overlays the experimental isotherm in the whole range of measured pressures, and the QSDFT pore size distribution shows a gradual transition from micro to mesoporosity.

The results for argon adsorption at 87.3 K are similar to those for nitrogen at 77.4 K. However, the monolayer transition in the NLDFT model occurs for argon at $P/P_0\sim2\times10^{-3}$ instead of $P/P_0\sim0.3\times10^{-3}$ that is characteristic to nitrogen. A typical example is given in Fig. 11 for a sample of CME2 carbon. As in the case of nitrogen adsorption, the QSDFT method allows one to eliminate the artificial layering transition inherent to the theoretical NLDFT isotherm (Fig. 11A), as well as the gap around 1nm on the pore size distribution curve (Fig. 11B). At the same time, the QSDFT and NLDFT pore size distributions agree well beyond the region around the layering transition.

It is important that the results of the QSDFT method obtained from nitrogen and argon isotherms are consistent, and the pore size distributions calculated using two different adsorbates agree well. This is demonstrated in Fig. 12, which shows the results of calculations granular active carbon Calgon F400, which is used in water treatment processes and is one of the most studied carbon materials.

An instructive example of micro-mesoporous materials is presented in Fig. 13. The adsorption isotherms of nitrogen and argon isotherms on CMC-2 carbon from Norit (Fig. 13A) are characterized by H4 type hysteresis loops (according to IU-

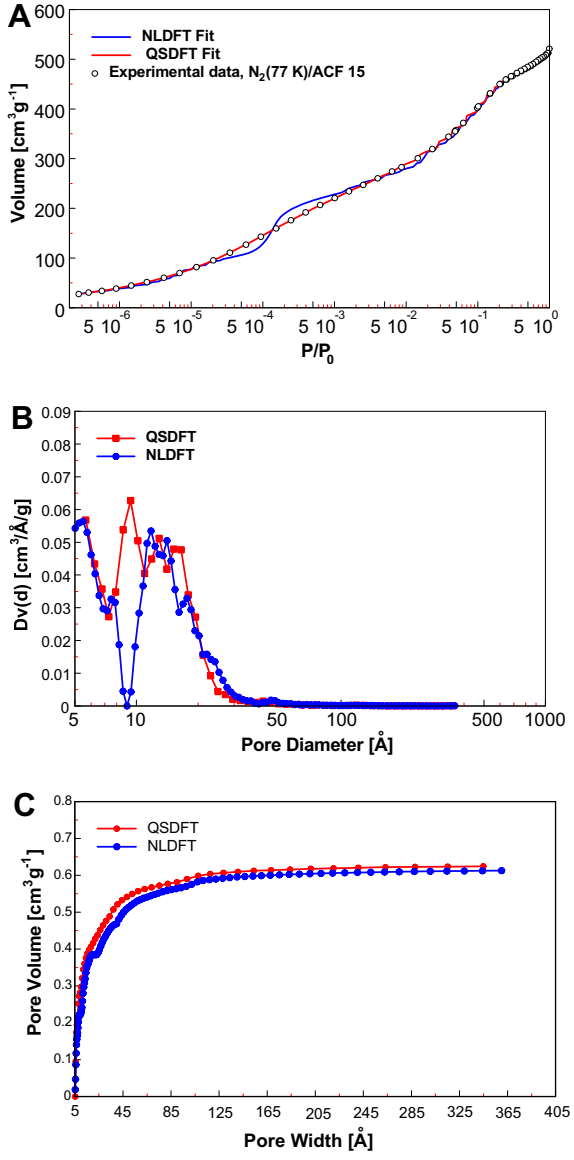

Fig. 9 – Comparison of the QSDFT and NLDFT methods for nitrogen adsorption for activated carbon fiber ACF-15 (sample obtained from Osaka Gas, Japan). (A) Experimental isotherm (in semi-logarithmic scale) together with the NLDFT and QSDFT theoretical isotherms. (B) NLDFT and QSDFT differential pore size distributions. (C) NLDFT and QSDFT cumulative pore volume distributions.

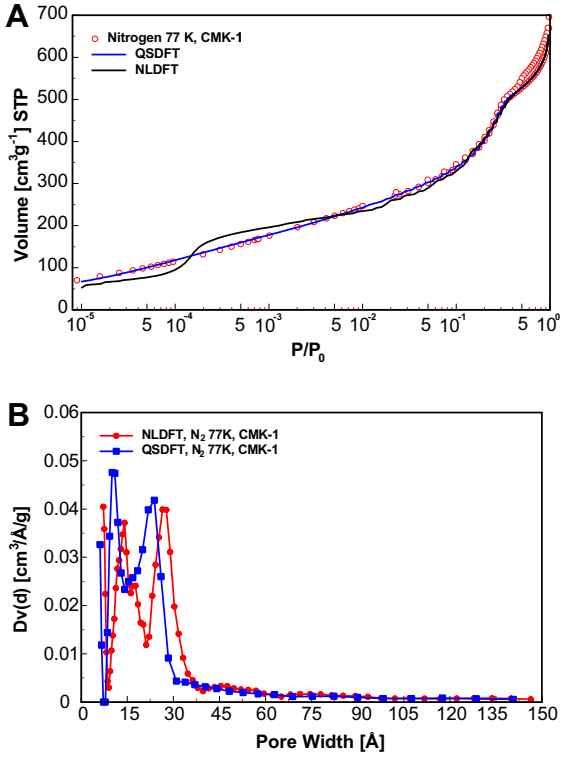

Fig. 10 – Comparison of the QSDFT and NLDFT methods for nitrogen adsorption for micro-mesoporous carbon CMK-1. (A) Experimental isotherm (in semi-logarithmic scale) together with the NLDFT and QSDFT theoretical isotherms. (B) NLDFT and QSDFT differential pore size distributions.

PAC [44]). This type of hysteresis suggests that mesopores in the CMC-2 carbon are embedded into a microporous framework, i.e. they are only accessible through the micropores. Evaporation of the capillary condensed liquid occurs therefore with a delay (due to cavitation [45]), and the mesopore size distribution in the region of hysteresis should be calculated from the adsorption branch. Although the prominent step characteristic to the monolayer transition on the theoretical NLDFT isotherm is completely eliminated on the theoretical QSDFT isotherm (Fig. 13B), the pore size distribution possesses a gap around 1 nm (Fig. 13C). Here, the gap on the pore size distribution around 1 nm is real; it reflects reveals a genuine bimodal structure with micropores <~1 nm and mesopores >~2 nm. This conclusion is supported by a perfect agreement between the pore size distributions calculated from nitrogen and argon isotherms.

5. Conclusions

We presented a new QSDFT model of adsorption on micro-mesoporous carbons. The main feature of the QSDFT model consists in a quantitative account of the surface geometrical inhomogeneity in terms of the roughness parameter. The roughness parameter represents the half-width of the extent of molecular level corrugations of pore wall surfaces. In general, it depends on the carbon source, procedure of synthesis, and degree of carbonization and chemical functionalization. The roughness parameter can be determined from the comparison of the theoretical and experimental adsorption isotherms on a reference surface and can be customized for a given type of carbon. The proposed QSDFT method provides a significant improvement over the traditional DFT methods, which assume the pore walls as homogeneous graphite-like plane surfaces. We show that this assumption of "mathematically" smooth pore boundaries ignores the inherent heterogeneity of real carbon surfaces and causes artificial layering transitions on theoretical isotherm, which lead to the gaps on the pore size distributions calculated from the comparison of commonly

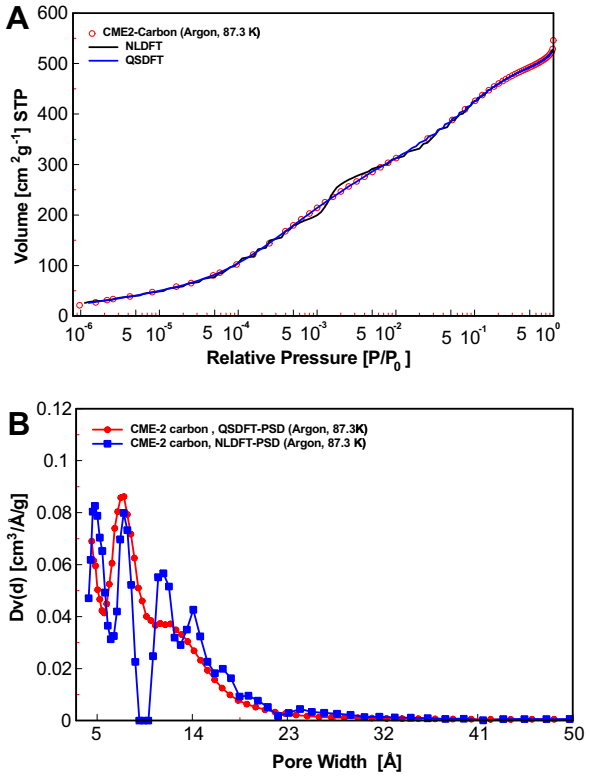

Fig. 11 – Comparison of the QSDFT and NLDFT methods for argon adsorption at 87.3 K on CME2 carbon. (A) Experimental isotherm (in semi-logarithmic scale) together with the NLDFT and QSDFT theoretical isotherms. (B) NLDFT and QSDFT differential pore size distributions.

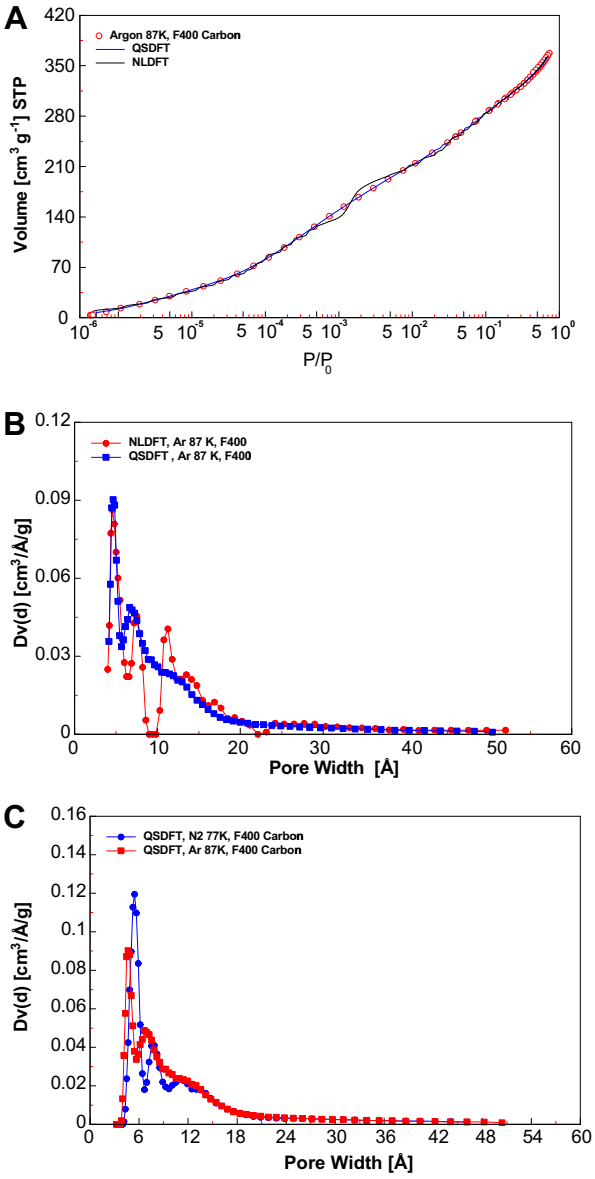

Fig. 12 – Pore size distribution calculations for granular activated carbon Calgon F 400. (A) experimental argon isotherm (in semi-logarithmic scale) together with the NLDFT and QSDFT theoretical isotherms. (B) NLDFT and QSDFT differential pore size distributions calculated from argon isotherm. (C) comparison of the QSDFT differential pores size distributions calculated from nitrogen and argon isotherms.

smooth experimental isotherms with step-wise theoretical isotherms. In this work, we have chosen the roughness parameter of 0.13 nm from the reference nitrogen (77.4 K) isotherm on a sample of Cabot BP-280 carbon black with a partial degree of graphitization, which was suggested as a suitable reference surface for a wide class of micro-mesoporous carbons [33,34]. We demonstrated that the theoretical isotherms calculated with the QSDFT model with the roughness parameter of 0.13 nm fit well experimental reference isotherms for both nitrogen and argon adsorption.

We developed the QSDFT models for pore size distribution calculations in the range of pore widths from 0.4 to 35 nm from nitrogen at 77.4 K and argon at 87.3 K adsorption isotherms. The QSDFT model improves significantly the method of adsorption porosimetry for heterogeneous carbons: the pore size distribution (PSD) functions do not possess artificial gaps in the regions of ~1 nm and ~2 nm, which are typical artifacts of the layering transitions in the standard NLDFT model. The QSDFT method is demonstrated on various microporous and micro-mesoporous carbons, including activated carbons fibers, coal based granular carbons, water purification adsorbents, and CMK-1 carbon templated on MCM-48 silica. It is shown that the QSDFT pore size distribution calculations from nitrogen and argon isotherms are consistent and that QSDFT and NLDFT agree outside the regions around the artificial gaps observed with NLDFT. Noteworthy, argon adsorption at 87.3 K provides a better resolution of pore sizes for ultra-micropores at higher vapor pressures than nitrogen adsorption.

It is worth noting that the proposed quantitative method for PSD calculating is based on the QSDFT model with the parameters corresponding to the Cabot BP-280 carbon black chosen as a reference. On principle, it is possible to customize the QSDFT model for different classes of carbons by choosing relevant reference surfaces for determining the model parameters, mainly the roughness parameter. However, the proposed model seems to be sufficient for practical purposes of a comparative analysis of different pore structures.

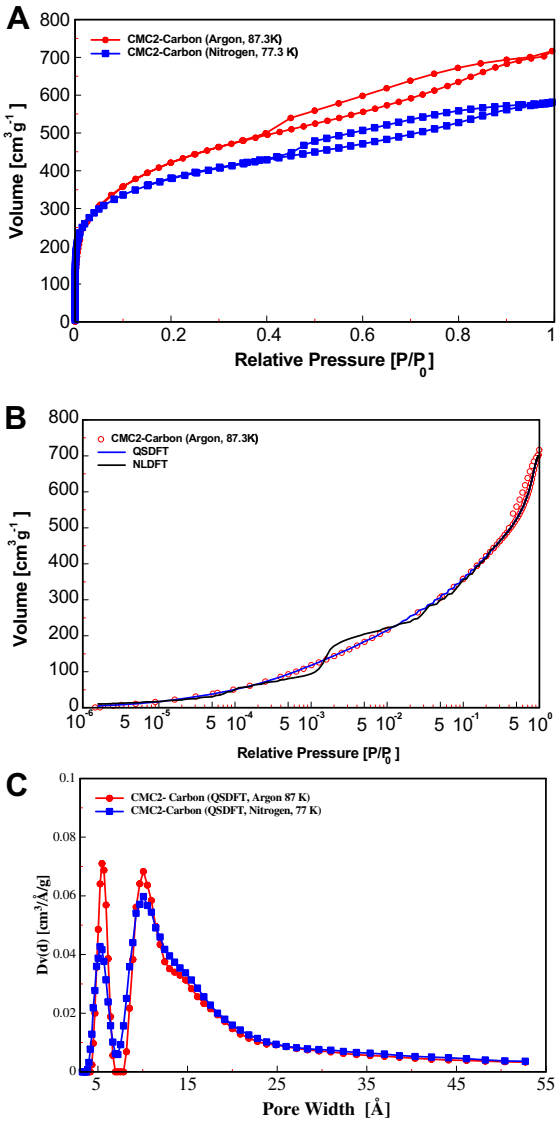

Fig. 13 – Pore size distribution calculations for micro-mesoporous Norit-CMC-2 carbon. (A) experimental nitrogen (77.4 K) and argon (87.3 K) adsorption isotherms. (B) Experimental argon (87.3 K) adsorption isotherm (in semi-logarithmic scale) together with NLDFT and QSDFT theoretical isotherms. (C) QSDFT differential pores size distributions obtained from nitrogen and argon isotherms.

Acknowledgments

The authors thank Prof. Catherine Morlay (University Lyon) for providing carbon samples used in water purification (CME2 and CMC2) and Prof. Michael Froeba (University of Hamburg) for providing the CMK-1 sample. AVN acknowledges partial support from the NSF ERC "Structured Organic Particulate Systems".

Appendix A. Supplementary data

Supplementary data associated with this article can be found, in the online version, at doi:10.1016/j.carbon.2009.01.050.

REFERENCES

[1] Evans R. Density functionals in the theory of nonuniform fluids. In: Henderson D, editor. Fundamentals of inhomogeneous fluids. New York: Marcel Dekker; 1992. p. 85–175.
[2] Neimark AV, Ravikovitch PI, Vishnyakov A. Bridging scales from molecular simulations to classical thermodynamics: density functional theory of capillary condensation in nanopores. J Phys: Condens Matter 2003;15:347–65.
[3] Wu JZ. Density functional theory for chemical engineering: from capillarity to soft materials. AIChE J 2006;52(3):1169–93.
[4] Evans R, Marconi UMB, Tarazona P. Capillary condensation and adsorption in cylindrical and slit-like pores. J Chem Soc Faraday Trans II 1986;82:1763–87.
[5] Peterson BK, Heffelfinger GS, Gubbins KE, van Swol F. Layering transitions in cylindrical pores. J Chem Phys 1990;93(1):679–85.
[6] Balbuena PB, Gubbins KE. Theoretical interpretation of adsorption behavior of simple fluids in slit pores. Langmuir 1993;9(7):1801–14.
[7] Ravikovitch PI, Vishnyakov A, Neimark AV. Density functional theories and molecular simulations of adsorption and phase transitions in nanopores. Phys Rev E 2001;64(1):011602.
[8] Neimark AV, Ravikovitch PI. Capillary condensation in MMS and pore structure characterization. Micropor Mesopor Mater 2001;44–45:697–707.
[9] Thommes M, Smarsly B, Groenewolt M, Ravikovitch PI, Neimark AV. Adsorption hysteresis of nitrogen and argon in pore networks and characterization of novel micro- and mesoporous silicas. Langmuir 2006;22(2):756–64.
[10] ISO-15901-3: Pore size distribution and porosity of solid materials by mercury porosimetry and gas adsorption – Part 3: Analysis of micropores by gas adsorption.,
[11] Seaton NA, Walton JPRB, Quirke N. A new analysis method for the determination of the pore-size distribution of porous carbons from nitrogen adsorption measurements. Carbon 1989;27(6):853–61.
[12] Lastoskie C, Gubbins KE, Quirke N. Pore size distribution analysis of microporous carbons: a density functional theory approach. J Phys Chem 1993;97(18):4786–96.
[13] Olivier JP, Conklin WB, Vonszombathely M. Determination of pore-size distribution from density functional theory – a comparison of nitrogen and argon results. Characterization of porous solid III. Studies Surf Sci Catal 1994;87:81–9.
[14] Maddox MW, Olivier JP, Gubbins KE. Characterization of MCM-41 using molecular simulation: heterogeneity effects. Langmuir 1997;13(6):1737–45.
[15] Olivier JP. Improving the models used for calculating the size distribution of micropore volume of activated carbons from adsorption data. Carbon 1998;36(10):1469–72.
[16] Ravikovitch PI, Vishnyakov A, Russo R, Neimark AV. Unified approach to pore size characterization of microporous carbonaceous materials from N_2, Ar, and CO_2 adsorption isotherms. Langmuir 2000;16(5):2311–20.
[17] Dash R, Chmiola J, Yushin G, Gogotsi Y, Laudisio G, Singer J, et al. Titanium carbide derived nanoporous carbon for energy-related applications. Carbon 2006;44:2489–97.
[18] Yushin G, Dash R, Jagiello J, Fischer JE, Gogotsi Y. Carbide-derived carbons: effect of pore size on hydrogen uptake and heat of adsorption. Adv Funct Mater 2006;16:2288–93.
[19] Fonseca DA, Gutierrez HR, Lueking AD. Morphology and porosity enhancement of graphite nanofibers through chemical etching. Micropor Mesopor Mater 2008;113:178–86.
[20] Coasne B, Hung FR, Pellenq RJM, Siperstein FR, Gubbins KE. Adsorption of simple gases in MCM-41 materials: the role of surface roughness. Langmuir 2006;22(1):194–202.

[21] Bandosz TJ, Biggs MJ, Gubbins KE, Hattori Y, Iiyama T, Kaneko K, et al. Molecular models of porous carbons. Chem Phys Carbon 2003;28:41–228.
[22] Yin YF, McEnaney B, Mays TJ. Dependence of GCEMC simulations of nitrogen adsorption on activated carbons on input parameters. Carbon 1998;36(10):1425–32.
[23] Ravikovitch PI, Jagiello J, Tolles D, Neimark AV. Extended abstracts of carbon conference, Lexington, KY; 2001.
[24] (a) Bhatia SK. Density functional theory analysis of the influence of pore wall heterogeneity on adsorption in carbons. Langmuir 2002;18(18):6845–56;
(b) Nguyen TX, Bhatia SK. Carbon 2005;43:775–85.
[25] Bakaev VA. Rumpled graphite basal plane as a model heterogeneous carbon surface. J Chem Phys 1995;102(3):1398–404.
[26] Turner AR, Quirke N. A grand canonical Monte Carlo study of adsorption on graphitic surfaces with defects. Carbon 1998;36(10):1439–46.
[27] Do DD, Do HD. Modeling of adsorption on nongraphitized carbon surface: GCMC simulation studies and comparison with experimental data. J Phys Chem B 2006;110(35):17531–8.
[28] Ustinov EA, Do DD, Fenelonov VB. Pore size distribution analysis of activated carbons: application of density functional theory using nongraphitized carbon black as a reference system. Carbon 2006;44:653–63.
[29] Ravikovitch PI, Neimark AV. Density functional theory model of adsorption on amorphous and microporous silica materials. Langmuir 2006;22:11171–9.
[30] Lowell S, Shields J, Thomas MA, Thommes M. Characterization of porous solids and powders: surface area, porosity and density. Springer; 2004.
[31] Kruk M, Li Z, Jaroniec M, Betz WR. Nitrogen adsorption study of surface properties of graphitized carbon blacks. Langmuir 1999;15:1435–41.
[32] Darmstadt H, Roy C. Comparative investigation of defects on carbon black surfaces by nitrogen adsorption and SIMS. Carbon 2001;39:841–8.
[33] Kruk M, Jaroniec M, Gadkaree KP. Nitrogen adsorption studies of novel synthetic active carbons. J Colloid Interf Sci 1997;192:250–6.
[34] Gardner L, Kruk M, Jaroniec M. Reference data for argon adsorption on graphitized and nongraphitized carbon blacks. J Phys Chem B 2001;105(50):12516–23.
[35] Rosenfeld Y. Free-energy model for the inhomogeneous hard-sphere fluid mixture and density-functional theory of freezing. Phys Rev Lett 1989;63(9):980–3.
[36] Yu YX, Wu JZ. Structures of hard sphere fluids from a modified fundamental measure theory. J Chem Phys 2002;117:10156–64.
[37] Roth R, Evans R, Lang A, Kahl G. Fundamental measure theory for hard-sphere mixture revisited: the white bear version. J Phys: Condens Matter 2002;14:12063–78.
[38] Rosenfeld Y, Schmidt M, Löwen H, Tarazona P. Fundamental-measure free-energy density functional for hard spheres: dimensional crossover and freezing. Phys Rev E 1997;55(4):4245–63.
[39] Ravikovitch PI. PhD thesis, Yale University; 1998.
[40] Lawson CL, Hanson RJ. Solving least squares problems. Philadelphia: SIAM; 1995.
[41] Hansen PC. Analysis of discrete ill-posed problems by means of the L-curve. SIAM Rev 1992;34(4):561–80.
[42] Jun S, Joo S, Ryoo R, Kruk M, Jaroniec M, Liu Z, et al. Synthesis of new, nanoporous carbon with hexagonally ordered mesostructure. J Am Chem Soc 2000;122:10712–3.
[43] Huwe H, Fröba M. Iron (III) oxide nanoparticles within the pore system of mesoporous carbon CMK-1: intra-pore synthesis and characterization. Micropor Mesopor Mater 2003;60(1–3):151–8.
[44] Sing KSW, Everett DH, Haul RAW, Mouscou L, Pierotti RA, Rouquerol J, et al. Reporting physisorption data for gas solid systems with special reference to the determination of surface-area and porosity (recommendations 1984). Pure Appl Chem 1985;57(4):603–19.
[45] Ravikovitch PI, Neimark AV. Density functional theory of adsorption in spherical cavities and pore size characterization of templated nanoporous silicas with cubic and three-dimensional hexagonal structures. Langmuir 2002;18(5):1550–60.